Supporting information

Metal-induced progressive alteration of conducting states in memristors for implementing an efficient analog memory: A DFT-supported experimental approach

D. Das[†*], A. Barman[†], P. K. Sarkar[#], P. Rajput[‡], S.N Jha[‡], R. Hübner[§], D. Kanjilal[|], P. Johari[†*] and A. Kanjilal[†*]

[*]Corresponding author: dd209@snu.edu.in, priya.johari@snu.edu.in, aloke.kanjilal@snu.edu.in

[†]Department of Physics, School of Natural Sciences, Shiv Nadar University, NH-91, Dadri, Gautam Buddha Nagar, Uttar Pradesh 201 314, India

[#] Department of Applied Science and Humanities, Assam University Silchar, Assam 788 011, India

[‡] Beamline Development & Application Section, Bhabha Atomic Research Centre, Trombay, Mumbai-400085, India

[§]Helmholtz-Zentrum Dresden-Rossendorf, Bautzner Landstrasse 400, 01328 Dresden, Germany

[|]Inter-University Accelerator Centre, Aruna Asaf Ali Marg, New Delhi 110067, India

S1. Results of SRIM calculations:

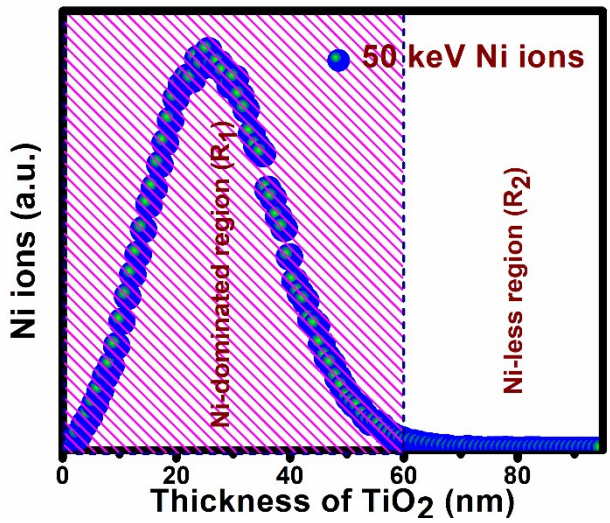

Fig S1. Doping profile of Ni ions in a 95 nm thick TiO_2 film.

The ion implantation was performed at the negative ion implanter beam facility (NIIBF), IUAC, India. Here, a sputter-based negative ion source mounted on a high-voltage (200 keV) stage is used to generate a negative ion beam. This ion source is facilitated with accelerated caesium ions and a cold cathode (in our case, it is Ni) to produce a negative ion beam of the cathode material. Such negative ion beam is guided and accelerated by the electrostatic quadrupole doublet and the high-electric field, respectively. Further, it is focused by an electrostatic quadrupole triplet and passed through a magnetic analyser, which maintains perpendicular transportation of the ion beam towards a high-vacuum implantation chamber loaded with A-TiO_2. During the implantation process, an electrostatic scanner was used to monitor the uniformity of the ion-beam scan. The interaction of the ion beam (Ni^-) with the solid (A-TiO_2) is determined by the energy of this incident beam. If the ion energy is high (~ MeV), then an inelastic collision with the electrons of the targeted solid may happen, leading to an excitation/ionization of the solid, known as electronic energy loss. However for low-incident energy (~ keV, like here in our case), the ions mostly lose their energy to the target atoms (in particular, the nuclei) of the solid via elastic collisions (known as nuclear energy loss), and a small displacement of the target atoms from its equilibrium position can be

observed. Such atomic displacements are very necessary for engineering electrical and structural changes in the targeted solid. During the energy loss of the incident ion, it can also gain some electrons from different shells of the target atoms, and eventually, a sluggish atom passes through the solid. As a result, it modifies the targeted solid to a desired precision in a well-controlled manner, and this is specifically effective for low-concentration doping engineering. In this context, the incident ion beam energy determines its penetration depth inside the solid (such penetration depth was predicted by the Stopping and Range of Ions in Matter (SRIM) calculations, before doing the experiment, as shown in Fig S1 in ESI). This is significant for choosing the dopant distribution across the thickness of the thin solid films, perhaps one of the most efficient technique. The doping concentration is controlled by the ion fluence (i.e. the number of ions that hit the target per unit area). The relation between the atomic concentration (in at.-%) and the ion fluence is given below. A typical calculation of the doping concentration for an ion fluence of 3×10^{15} ions/cm^2 is also provided.

$$Atomic\ \% = \frac{Fluence \times 100\ \%}{n \times t}$$

Here n is the number of atoms/ cm^3, for TiO_2 it is 3.98×10^{22} atoms/ cm^3 and t is the thickness of the film (~ 95 nm). Thus, the Ni-at % is ~ 0.8, which is very close to the one used in the DFT simulations (~ 0.9 at %). Here, Ni is used as a dopant in *A*-TiO_2 due to its well-known ability of trap states enclosure. [1, 2] The difference of chemical valence between Ti and Ni is the main reason behind the formation of trap states. [1, 2] By using such trap states we could able to demonstrate the gradual tuning of the conductance states, especially the LCS region of the AS, as evidenced from our *I-V* measurements (See Fig 1b). In addition, Ni-improves the short-term memory loss and modifies the local electrostatic barriers to stimulate modulatory action for LTP.

S2. *I-V* characteristics of pristine device

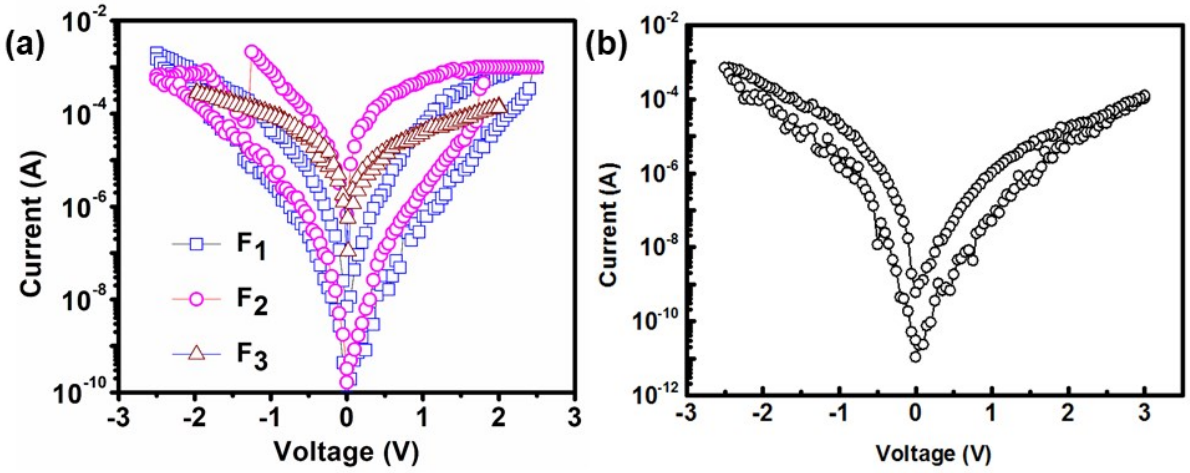

Fig S2. I-V characteristics of the (a) F_1, F_2, and F_3 samples **(**b**)** The pristine (Au/*A*-TiO_2/Pt) device (F_0).

S3. LCS and HCS distribution

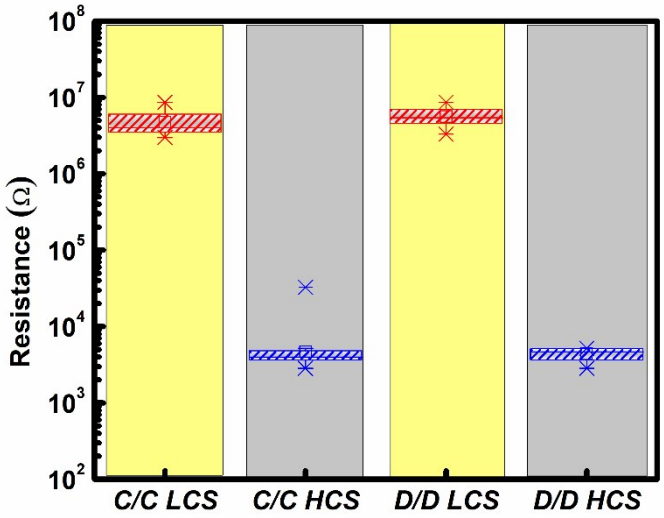

Fig S3. LCS and HCS distribution for different cycle-to-cycle (C/C) and device to-device (D/D) operations. It illustrates an average LCS/HCS ratio of 10^3.

S4. Variation of SET and RESET voltages

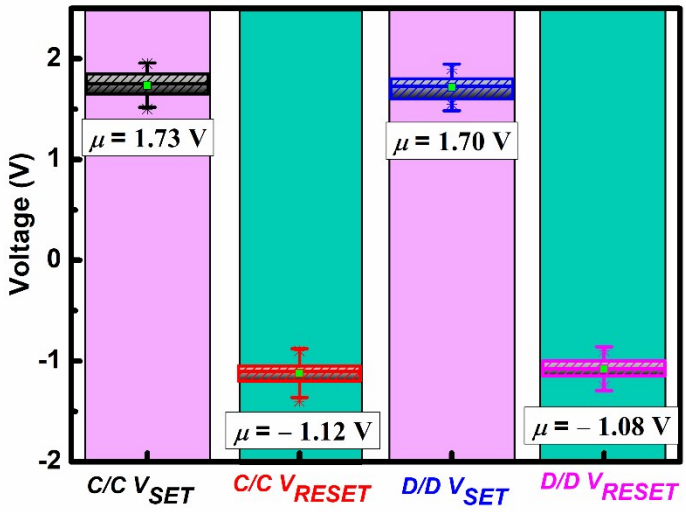

Fig S4. Variation of SET and RESET voltages for different cycle-to-cycle (C/C) and device to-device (D/D) operations.

S5. Ni-doping proportion

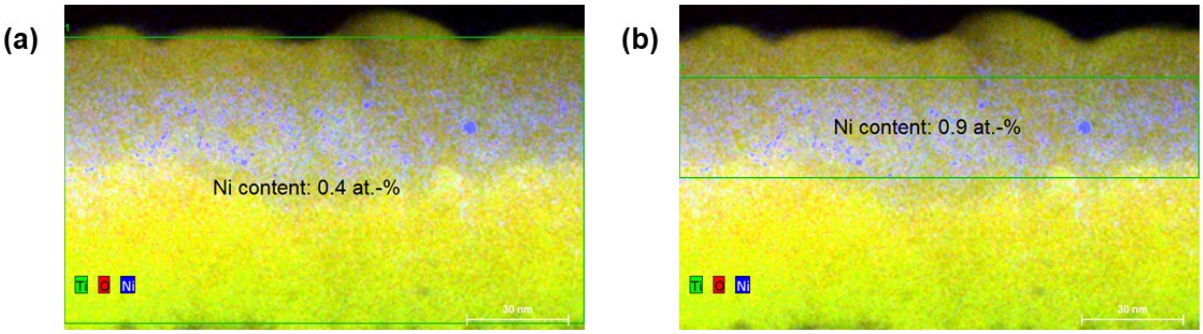

Fig S5. (a) Overall Ni-doping of 0.4 at.% considering the whole TiO_2 film marked with a green rectangle and **(**b**)** doping proportion at the Ni-active R_1 region (0.9 at.%). These analyses were done with the help of the Bruker Esprit 1.9 software.

S6. Structural parameters extracted from XAFS measurements

Table S6. Structural parameters obtained from fitting of the Ti *K*-edge XAFS spectra, where *N* is the coordination number, *R* is the bond distance, and σ^2 is the Debye-Waller factor. The numbers in parentheses indicate the standard deviations.

		Standard *A*-TiO_2		Ni: *A*-TiO_2	
Path	*N*	*R* (Å)	σ^2 (Å^2)	*R* (Å)	σ^2 (Å^2)
O (1st/2nd)	6	1.972 (3)	0.0143 (3)	1.978 (5)	0.0169 (5)

Ti (3^{rd})	4	3.086 (4)	0.0149 (5)	2.946 (5)	0.0182 (4)
Ti (4^{th})	4	3.494 (6)	0.0143 (4)	3.429 (8)	0.0145 (9)
O (1^{st}/2^{nd}) Ti (fourth)	8	3.608 (7)	0.0178 (5)	3.496 (8)	0.0142 (8)

X-ray absorption near edge spectroscopy (XANES) and extended X-ray absorption fine structure (EXAFS) measurements of Ni:*A*-TiO_2 and standard *A*-TiO_2 samples at the Ti-*K* edge were recorded in fluorescence mode using a Vortex detector at the Scanning XAFS beamline (BL-9) at the Indus-2 Synchrotron Source at the Raja Ramanna Centre for Advanced Technology (RRCAT), Indore, India. The energy range was calibrated using Ti and Ni foils. The XAFS data were analyzed using the FEFF 6.0 code, [3] which includes background reduction and Fourier transform to derive the versus *R* spectra from the absorption spectra (using ATHENA software), generation of the theoretical XAFS spectra starting from an assumed crystallographic structure and finally fitting of experimental data with the theoretical spectra using ARTEMIS software. [4]

S7. Structure of Ni-substituted *A*-TiO_2 (Ni_{Ti})

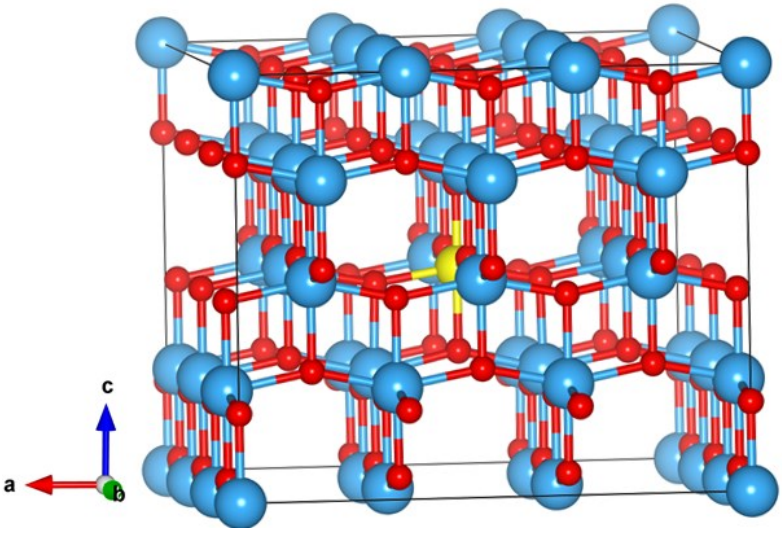

Fig S7. DFT-simulated structure of Ni-substituted *A*-TiO_2, where the substitutional Ni-site (Ni_{Ti}) is marked by a yellow ball; blue and red balls represent titanium and oxygen atoms, respectively.

S8. Density of states (DOS) of Ni_{Ti}

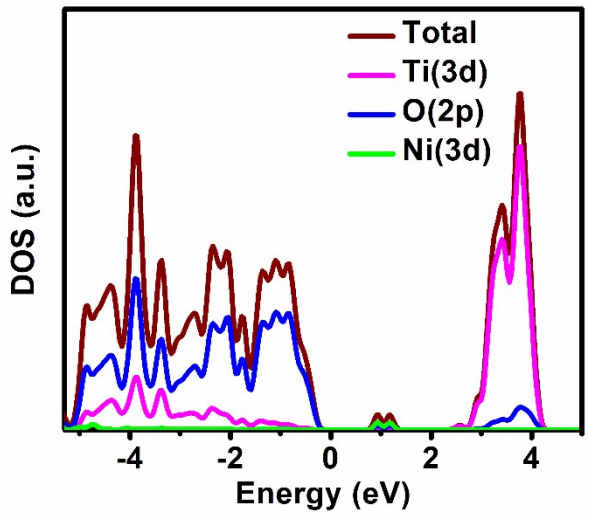

Fig S8. Projected density of states of $Ni_{Ti.}$ Here brown, magenta, blue, and green coloured lines represent the total DOS at the Ti-3*d*, O-2*p*, and Ni-(3*d*) orbitals, respectively. For DOS plotting, we refer the position of the valence band maximum with respect to the pure *A*-TiO_2.

References

(1) Z. Zhaohui, M. Li, and L. Guo, *Journal of Physics and Chemistry of Solids,* 2010, **71**,1707-1712.

(2) P. Haowei, J. Li, S. Li, and J. Xia, *Journal of Physics: Condensed Matter,* 2008, **20**, 125207.

(3) S. I. Zabinsky, J. J. Rehr, A. Ankudinov, R. C. Albers, M. J. Eller, *Physical Review B***,** 1995*,* **52**, 2995-3009.

(4) B. Ravel, M. Newville, Athena, Artemis, *Journal of Synchrotron. Radiation.,* 2005**,** **12**, 537-541.